

A Bayesian approach for inverse potential problem with topological-Gaussian prior

Zhiliang Deng*¹, Xiaofei Guan², Haiyang Liu¹, Zhiyang Wang², and
Xiaomei Yang³

¹University of Electronic Science and Technology of China

²Tongji University

³Southwest Jiaotong University

April 3, 2025

Abstract

This paper addresses the reconstruction of a potential coefficient in an elliptic problem from distributed observations within the Bayesian framework. In such problems, the selection of an appropriate prior distribution is crucial, particularly when the function to be inferred exhibits sharp discontinuities, as traditional Gaussian priors often prove inadequate. To tackle this challenge, we develop the topological prior (TP), a new prior constructed using persistent homology. The proposed prior utilizes persistent pairs to characterize and record the topological variations of the functions under reconstruction, thereby encoding prior information about the structure and discontinuities of the function. The TP prior, however, only exists in a discretized formulation, which leads to the absence of a well-defined posterior measure in function spaces. To resolve this issue, we propose a TP-Gaussian hybrid prior, where the TP component detects sharp discontinuities in the function, while the Gaussian distribution acts as a reference measure, ensuring a well-defined posterior measure in the function space. The proposed TP prior demonstrates effects similar to the classical total variation (TV) prior but offers greater flexibility and broader applicability due to three key advantages. First, it is defined on a general topological space, making it easily adaptable to a wider range of applications. Second, the persistent distance captures richer topological information compared to the discrete TV prior. Third, it incorporates more adjustable parameters, providing enhanced flexibility to achieve robust numerical results. These features make the TP prior a powerful tool for addressing inverse problems involving functions with sharp discontinuities.

*dengzhl@uestc.edu.cn

1 Introduction

The inverse potential problem we study in the paper is governed by the elliptic equation

$$\begin{cases} -\Delta u + qu = f, & \text{in } \Omega, \\ u = 0 & \text{on } \partial\Omega, \end{cases} \quad (1)$$

where $\Omega \subset \mathbb{R}^s$ ($s = 1, 2$) is a bounded open domain, and the function f is the known source term. The potential q belongs to the admissible set K defined as

$$K = \{q \in L^\infty(\Omega) : c_0 \leq q(x) \leq c_1 \text{ a.e. in } \Omega\}, \quad (2)$$

with $0 \leq c_0 < c_1 < \infty$. We collect the observational data of the solution $u(x)$ to (1) on Ω by

$$u^\eta(x) = u(x) + \eta(x), \quad x \in \Omega, \quad (3)$$

where η denotes the measurement noise. The inverse potential problem aims to estimate the potential function q from the noisy observation u^η . This issue frequently arises in practical applications such as quantitative dynamic elastography [10], which focuses on estimating tissue parameters from tissue displacement measurements. In [1], G. Bal and G. Uhlmann discussed the reconstruction of an absorption coefficient in the photoacoustic tomography problem by the internal observation data in a scattering medium. In some real-world cases, the inverse potential problem is also inherently linked to time-dependent phenomena, e.g., the reconstruction of the radiativity coefficient in heat equation [1, 28, 35, 39, 41] and the reconstruction of the potential in Schrödinger equation [3, 4]. Due to their wide-ranging real-world applications, inverse potential problems have garnered significant attention from researchers.

From a theoretical perspective, the uniqueness and conditional stability of the inverse potential problem have been extensively investigated, as seen in works such as [1, 28]. These studies explore conditions under which the solution is unique and stable with respect to perturbations in the data. In terms of numerical methods, the inherent difficulty arises from the problem's ill-posed nature, which presents significant challenges in constructing accurate and stable numerical approximations. The ill-posedness, characterized by high sensitivity to noise and the potential for non-uniqueness, necessitates the development of specialized regularization techniques and robust algorithms to achieve reliable and meaningful results. Extensive work has been devoted to overcoming these challenges, with two dominant methodological strands emerging: (1) regularization approaches, including Tikhonov regularization [5, 19, 20, 27], and (2) statistical inference techniques, notably Bayesian methods [11, 31–33, 37, 38]. Tikhonov regularization, in particular, has been widely applied to solve inverse potential problems, providing a means to recover numerical stability by incorporating prior information to regularize the solution [19, 28]. This method has demonstrated considerable success in improving the stability of numerical solutions, particularly when dealing with noisy or incomplete data. On the other hand, the Bayesian approach offers a more flexible framework for incorporating uncertainties in the problem, providing probabilistic solutions that account for both data and model uncertainties. The theoretical guarantees of Bayesian inversion - particularly its well-posedness as shown in [11, 37] - explain why this approach has become fundamental to solving inverse problems. In [32, 33], J. Latz extended the well-posedness results

with minimal constraints on the likelihood functions and priors, offering an in-depth discussion of well-posedness across multiple metrics, such as the Hellinger distance, total variation, weak topology, and Wasserstein metric. With the advancement of theoretical frameworks, the Bayesian approach has also achieved remarkable success in the application to inverse problems, e.g., the inverse scattering problems [8, 9, 21, 24, 30, 34]. The Bayesian approach has proven highly effective in inverse scattering problems, allowing for the characterization of the posterior distribution of the obstacle object [8, 9, 34] or the refractive index [21, 24, 30] based on scattered field data. Similarly, the problem of reconstructing conductivity parameters in elliptic equations has been widely explored through Bayesian inversion [6, 11, 22, 37]. The prior distribution is a critical component of Bayesian inversion, as it encodes prior beliefs or information about the unknowns. Its role is comparable to that of the regularizer in regularization-based approaches. Some studies focus on the topic of constructing an appropriate prior distribution, e.g., a rich class of priors derived from the Markov random fields [2, 26]. In [40], an l_1 prior including the TV prior and the Besov space $B_{1,1}^s$ prior is constructed to deal with less regularity unknown parameters. In [42], a TV-Gaussian hybrid prior is presented for detecting sharp jumps of the object function. The geometry information prior is discussed for the geometry object reconstruction problem in [9, 25]. The priors are almost all based on analytical methods, imposing regularity conditions on the unknown functions.

While Bayesian inference has achieved notable success across diverse inverse problems, inverse potential problems have received limited attention within this framework. The method's inherent advantages in uncertainty quantification and solution stability suggest it will emerge as an increasingly important tool for this problem class. In this paper, we provide a survey of the application of the Bayesian method to the inverse potential problem. Our main contribution is the proposal of a new prior based on the topological tool of persistent homology. This prior aims to constrain the topological variation of the unknown, thereby imparting a degree of smoothness. It can be demonstrated that the new prior serves a similar role to that of the classical TV prior. It should be noted that the proposed TP prior differs from that in [9]. In [9], the primary focus is on the geometric shape. In contrast, our method emphasizes the topological structure inherent in the unknown functions. These topological features are encoded in the so-called persistence diagrams, which allow us to extract and analyze the latent shape information. This new prior introduces a fresh viewpoint for understanding the unknown functions. We present several numerical examples to illustrate the effectiveness of the proposed prior. Through comprehensive numerical experiments, we demonstrate that our approach achieves substantially better performance than Gaussian priors for non-smooth function estimation, particularly in cases involving abrupt changes (e.g., sharp jumps or step discontinuities). Furthermore, in line with the theoretical insights from [43], the TP-based prior exhibits behavior similar to that of TV-based priors [42], as evidenced by the numerical results. We emphasize the key distinctions: (a) The TP-based prior is defined on a general topological space that preserves richer topological information, substantially expanding its potential applications across multiple domains; (b) The TP-based prior enables more robust results with greater ease, owing to its increased number of adjustable parameters compared to the TV-based prior.

This paper is organized as follows: In Section 2 we present the necessary background on persistent homology; In Section 3 we discuss the Bayesian approach with TP-Gaussian hybrid prior; In Section 4 we present our numerical examples and results. Lastly in Section

5 we give some conclusions.

2 Persistent homology

This section introduces necessary background knowledge on persistence diagram and persistent homology which forms a concrete basement for our prior. For more details one can refer to [43, 44].

We consider a space (object) X that varies as a function of a parameter r . When the parameter is fixed at a specific value \tilde{r} , homology groups characterize the essential topological features of $X(\tilde{r})$, providing a means to classify k -dimensional holes in $X(\tilde{r})$. Persistent homology captures the changes in the shape of this object as the parameter r varies. Actually, when the parameter r changes until a certain critical value is reached, the topology of the object also undergoes changes. We can observe the birth of new k -dimensional holes and the death of existing ones. The birth time $r = b$ of a k -dimensional hole is recorded, as is the death time $r = d$. The persistence of this k -dimensional hole is denoted as $d - b$. This dynamic process can be illustrated by what is known as a filtration process.

For simplicity, we assume that the object X is a simplicial complex that is homeomorphic to a specific geometric object, typically its triangulation X . We suppose that X has $m + 1$ vertices $\{p_0, \dots, p_m\} \subset \mathbb{R}^d$. A simplicial complex is a set composed of basic cells, including points, line segments, triangles, and their n -dimensional counterparts, constructed from the subsets of $\{p_0, \dots, p_m\}$. These cells, referred to as simplices, are organized in a way that respects the combinatorial structure of the complex, where each cell is defined by its vertices and is associated with lower-dimensional cells that form its boundary. Specifically, a k -dimensional simplex σ , or k -simplex, $k \leq m$, is the set of convex combinations of $k + 1$ affinely independent points $\{p_0, p_1, \dots, p_k\}$, i.e.,

$$\sigma = \left\{ \sum_{i=0}^k \lambda_i p_i \mid \sum_{i=0}^k \lambda_i = 1 \text{ and } \lambda_i \geq 0 \right\}. \quad (4)$$

The points p_0, p_1, \dots, p_k are called the vertices of σ and the number k the dimension of σ . We denote the simplex as $\langle p_0, \dots, p_k \rangle$, i.e., $\sigma = \langle p_0, \dots, p_k \rangle$. Any simplex spanned by a subset of $\{p_0, p_1, \dots, p_k\}$ is called a face of σ . If τ is a face of σ , then σ is a coface of τ . With the concept of simplices, we can define the simplicial complex X in \mathbb{R}^d as a (finite) collection of simplices such that:

- i. any face of a simplex of X is a simplex of X ;
- ii. the intersection of any two simplices of X is either empty or a common face of both.

We denote the set generated by k -simplices of X over the binary field \mathbb{Z}_2 as $C_k = C_k(X)$. It consists of all k -chains as

$$\mathbf{c} = \sum_j \gamma_j \sigma_j, \quad (5)$$

where γ_j are 0 or 1 and σ_j are k -simplices in X . The addition over \mathbb{Z}_2 for two k -chains is defined by $\mathbf{c} + \tilde{\mathbf{c}} = \sum_j (\gamma_j + \tilde{\gamma}_j) \sigma_j$, where $\mathbf{c} = \sum_j \gamma_j \sigma_j$ and $\tilde{\mathbf{c}} = \sum_j \tilde{\gamma}_j \sigma_j$. The k -chains

in C_k form a group under this addition, which we denote as $(C_k, +)$ and refer to as the group of k -chains.

Different types of chains in X are distinguished by homology group, which is defined by virtue of the quotient group. To establish this, we need to introduce the concepts of boundary and boundary operator. The boundary of a k -simplex $\sigma = \langle p_0, \dots, p_k \rangle$ can be viewed as its geometric boundary, which is the sum of all its $(k-1)$ -faces, given by:

$$\partial_k \sigma = \sum_{i=0}^k (-1)^i \langle p_0, \dots, \hat{p}_i, \dots, p_k \rangle = \sum_{i=0}^k \langle p_0, \dots, \hat{p}_i, \dots, p_k \rangle, \quad (6)$$

where \hat{p}_i indicates that the vertex p_i is omitted. The operator ∂_k is called the boundary operator. Then the boundary of a k -chain $\mathbf{c} = \sum_j \gamma_j \sigma_j$ (σ_j is k -simplex) is the linear combination of boundaries of its k -simplices

$$\partial_k \mathbf{c} = \sum_j \gamma_j \partial_k \sigma_j, \quad \gamma_j \in \mathbb{Z}_2. \quad (7)$$

The boundary operator ∂_k maps a k -chain group C_k to a $(k-1)$ -chain group C_{k-1} . It induces the corresponding group homomorphisms, and the kernels and images of these homomorphisms can be used to construct quotient groups. Furthermore, each quotient group provides a means to distinguish two special types of chains: k -cycles and k -boundaries. For clarity, we give the definition of the kernel and image of the homomorphism ∂_k

$$\begin{aligned} \text{Ker}(\partial_k) &:= \{ \mathbf{c} \in C_k \mid \partial_k \mathbf{c} = 0 \}, \\ \text{Im}(\partial_k) &:= \{ \partial_k \mathbf{c} \mid \mathbf{c} \in C_k \}. \end{aligned} \quad (8)$$

A k -cycle is a k -chain with empty boundary, i.e., $\partial_k \mathbf{c} = 0$. The kernel $\text{Ker}(\partial_k)$ is composed of all k -cycles and is a subgroup of C_k , denoted by Z_k . A k -boundary \mathbf{c} is a k -chain which is the boundary of a $(k+1)$ -chain \mathbf{a} , i.e., $\mathbf{c} = \partial \mathbf{a}$. Similarly, all k -boundaries form a subgroup $B_k = \text{Im}(\partial_{k+1})$ of the chain group C_k . According to the fundamental property for the homology procedure: For all integers k and every $(k+1)$ -chain \mathbf{a} , we have $\partial_k \partial_{k+1} \mathbf{a} = 0$. Therefore, we know that a k -boundary is necessarily a k -cycle. In other words, a k -boundary group B_k is a subgroup of the k -cycle group Z_k . But the reverse does not hold, i.e., a k -cycle is not necessarily a k -boundary. To distinguish those non-boundary k -cycles, the notion of homology group is a powerful tool as follows: The k -th homology group of the object X is defined by the quotient $H_k(X) = Z_k(X)/B_k(X)$, whose element is a collection of k -chains obtained by adding k -boundaries from B_k to a given k -cycle, $\mathbf{c} + B_k$ with $\mathbf{c} \in Z_k$. We call $\mathbf{c} + B_k$ a class of H_k and use \mathbf{c} as the representative of this class. It is evident that the groups Z_k , B_k , and H_k are linear spaces, as their coefficients are taken from the binary field \mathbb{Z}_2 . The ranks of these homology group are given by the base 2 logarithm of their cardinalities, specifically:

$$\text{rank}(H_k) = \log_2(\text{card}(H_k)).$$

The rank of the k -homology group, $\text{rank}(H_k)$, is called the k -Betti number of Z_k . And we have the relation $\text{rank}(H_k) = \text{rank}(Z_k) - \text{rank}(B_k)$. The k -Betti number measures the number of k -dimensional holes of the complex X .

Homology groups provide a static characterization of the topology of a simplicial complex. For a specific r , the topology of X can be analyzed using homology tools.

However, we often need to investigate the topological changes that occur as the object X varies with r . It is evident that the homology group alone cannot capture these dynamic topological changes. When the evolution of X follows a certain law, we can use persistent homology to record the persistence of specific homology classes during this process. Filtration is introduced to describe this law, resulting in a sequence of subcomplexes of the simplicial complex X

$$\emptyset = X_{r_0} \subseteq X_{r_1} \subseteq \cdots \subseteq X_{r_n} = X.$$

In practical scenarios, our emphasis is not on the specific value of r , but rather on the state itself. Therefore, the filtration is denoted as

$$\emptyset = X_0 \subseteq X_1 \subseteq \cdots \subseteq X_n = X. \quad (9)$$

The corresponding sequence of sets $\{\mathbf{c}_0, \dots, \mathbf{c}_{n-1}\}$ with the property that $X_{j+1} = X_j \cup \mathbf{c}_j$ for $j = 0, \dots, n-1$ is called a filter. A complex X with a filtration is called a filtered complex, denoted by \mathcal{X} . By definition, for a simplex $\sigma \in X_i$, it holds that $\sigma \in X_j$ for $j = i, \dots, n$. The birth time $b(\sigma)$ of a simplex σ in the filtration is defined as the smallest index i such that $\sigma \in X_j$ if and only if $j \geq b(\sigma)$. We use the simple elliptic curve $y^2 = x^3 - x$ (Figure 1(left)), where $x \in [-1, 2]$, as an example to illustrate the concept of filtration. Some samples are collected along the curve and a complex is constructed using these samples, as shown in Figure 1. A filtration of the complex is illustrated in Figure 2. It is important to note that different filtrations exist for some complexes. The commonly used filtrations include the Vietoris-Rips complex, Čech complex, sublevel filtration, lower-star filtration, and others [7, 12, 15, 23, 29, 44]. We here state the concept

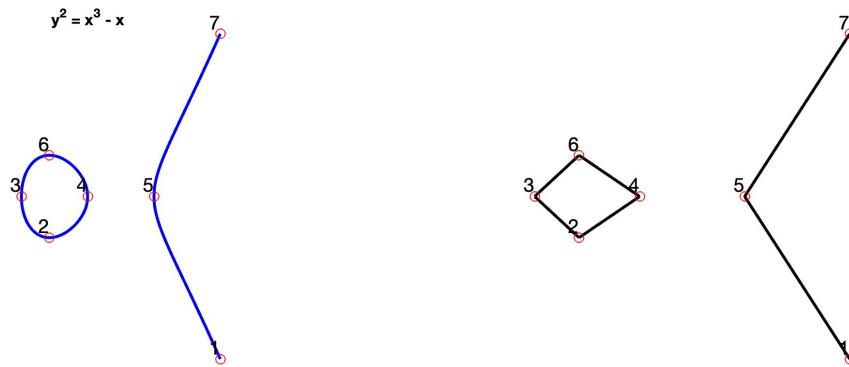


Figure 1: Elliptic curve (left) and a complex is constructed with the triangulation (right).

of lower star filtration (see [43, 44]). For a set U of vertices in X , its star is defined as the set of simplices that have at least one vertex in U , and its link as the set of faces of simplices in the star that do not also belong the star [43, 44]:

$$\begin{aligned} \text{St } U &= \{\sigma \in X \mid \exists p \in U, p \in \sigma\}, \\ \text{Lk } U &= \{\tau \in X \mid \tau \subseteq \sigma \in \text{St } U, \tau \notin \text{St } U\}. \end{aligned} \quad (10)$$

If we endow the vertices p in X with real values $h(p)$ from a function h , the vertices can be sorted along with their neighboring vertices in the star according to these values. We assume that h is a defined and non-degenerate function for all vertices p of the given

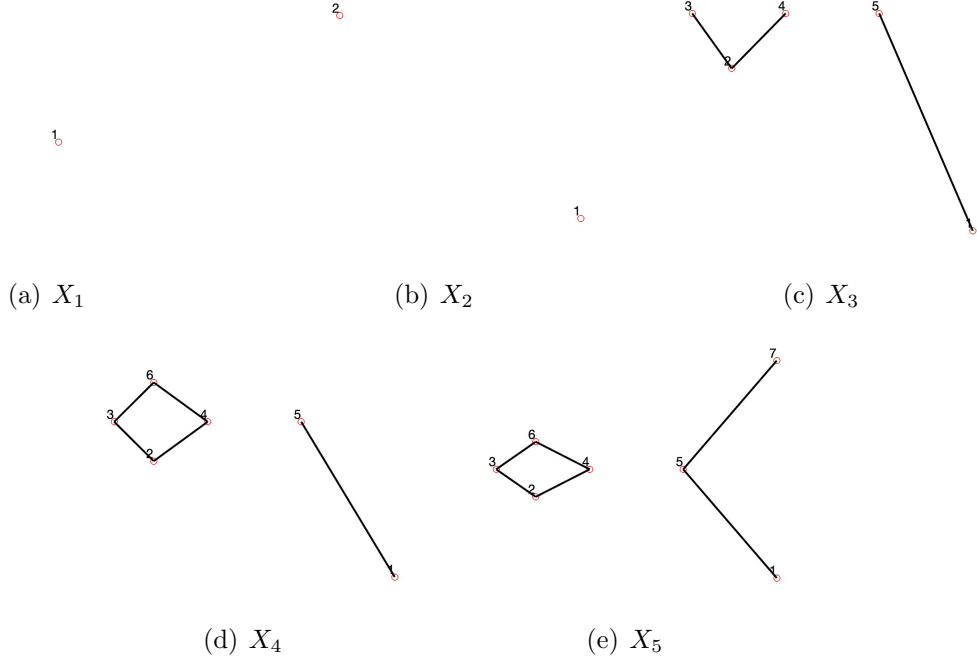


Figure 2: A filtration of Figure 1.

complex X , meaning that the function values are distinct for all vertices [16, 18, 43]. Following [43, 44], we use this function to define the lower star and the lower link of p ,

$$\begin{aligned} \text{St}_- p &:= \{\sigma \in \text{St } p \mid v \in \sigma \Rightarrow h(v) \leq h(p)\}, \\ \text{Lk}_- p &:= \{\sigma \in \text{Lk } p \mid v \in \sigma \Rightarrow h(v) \leq h(p)\}. \end{aligned} \quad (11)$$

For a simplicial complex X with endowed real function values $h(p_i)$ for each vertex, the sequence of all vertices $\{p_0, \dots, p_m\}$ can be ordered according to their increasing function values. Then the sequence of subcomplexes $\{\text{St}_- p_0, \dots, \text{St}_- p_m\}$ generates a filter that forms a filtration that is called lower star filtration of h . By examining the corresponding homology groups at each stage in this filtration, we can describe how long certain properties (classes) of the complex survive in the sequence. Typically, more emphasis is placed on how the number of homology classes (the Betti number) changes during the filtration, rather than on the exact structure of each homology group. Thus, examining a k -simplex that creates a new class alongside a $(k+1)$ -simplex that eliminates an existing class is sufficient to comprehend the topological changes. The core process involves tracking the moments when a new homology class emerges (is ‘born’) and when it becomes trivial or merges with another class. For a specific homology class, the birth time, denoted as b , and the death time, denoted as d , define its lifespan. We can use so-called persistence diagrams to illustrate the persistence of each k -dimensional hole.

In order to capture the variation of the Betti numbers of the homology groups at each stage of a given filtration, we assume that the filtration of X is complete. This means that each subcomplex X_{i+1} in the filtration is formed from X_i by adding exactly one simplex σ_i . The k -Betti number of a k -homology group increases by 1 when a new k -homology class is created, which occurs when a k -simplex σ_i with a certain property is added to the filtration. Such a simplex σ_i is referred to as positive. Conversely, the k -Betti number of the k -homology group decreases by 1 when a $(k+1)$ -simplex with a specific property (referred to as negative) is added to the filtration, which destroys a k -homology class.

We can analyze these properties by examining how the new simplex is connected to the preceding subcomplexes. For a given k -homology class that is created by a positive k -simplex at a certain stage r_i of the filtration and is destroyed by a $(k + 1)$ -simplex at a later stage r_j of the filtration, the corresponding k -simplex and the $(k + 1)$ -simplex can be “paired”. Their birth time difference in the filtration is called their persistence. The pair is called persistence pair. A formal algorithm for the pairing of simplices is described in [17, 43] (See Algorithm 1).

Algorithm 1 Pairing of simplices:

- 1: **Input:** X_i and σ_i , for $i = 1, \dots, n$.
 - 2: **Initialize:** $C = \emptyset$, $P_k = \emptyset$, for all possible k .
 - 3: **for** $j = 1, \dots, n$ **do**
 - 4: **if** σ_j with $\dim\sigma_j = k$ is positive and creates the cycle c_j ,
 - 5: then add c_j into C , i.e., $C = C \cup c_j$.
 - 6: **elseif** σ_j with $\dim\sigma_j = k + 1$ is negative and σ_j destroys c_{i_0} in C ,
 - 7: then form the pair (c_{i_0}, c_j) and add this pair into P_k .
 - 8: **end if**
 - 9: **Output:** P_k (as a multiset) of persistence pairs of dimension k in the given filtration.
 - 10: **end for**
-

Using the lower star filtration, it is also possible to pair the vertices. When both simplices of a pair lie in the same lower star, we call such a pair trivial. In this case, when using the (non-complete) lower star filtration, the corresponding cycle is created and destroyed simultaneously as the lower star set of the vertex is added to the filtration. This means that the existence of this class cannot be detected within the current “resolution” of the lower star filtration. As a result, we focus only on the nontrivial pairs, i.e., the nonlocal pairs (see Definition 2.1). In the following, we will pair vertices instead of simplices and use $P(\mathcal{X})$ to denote the collection of all pairs of vertices in \mathcal{X} .

Definition 2.1. Assume that (σ, τ) is a pair of simplices given by Algorithm 1, where $\sigma \in \text{St}_+ \sigma_s$ and $\tau \in \text{St}_- \sigma_t$. We say that σ and τ are locally paired if $s = t$ and they are non-locally paired if $s \neq t$.

Definition 2.2. Let (σ, τ) be a non-locally paired simplex pair, where $\sigma \in \text{St}_+ \sigma_s$ and $\tau \in \text{St}_- \sigma_t$. We define the corresponding persistence pair of vertices as (s, t) .

3 The TP-Gaussian prior

We describe the TP-Gaussian priors in this section. It should be pointed out here that the space $L^\infty(\Omega)$ is not separable, and its dual space has a relatively complex structure [13]. For simplicity, we embed the admissible set K to $L^2(\Omega)$.

First, we introduce the Gaussian measure on $L^2(\Omega)$. For every $\iota \in L^2(\Omega)^*$, if $\mu_0 \circ \iota^{-1}$ is a Gaussian measure on \mathbb{R} , then μ_0 is defined as a Gaussian measure on $L^2(\Omega)$. The covariance operator C_0 associated with μ_0 is given by:

$$C_0(\iota_1, \iota_2) = \int_{L^2(\Omega)} \iota_1(q)\iota_2(q) d\mu_0(q) - \mathbb{E}[\iota_1]\mathbb{E}[\iota_2], \quad \iota_1, \iota_2 \in L^2(\Omega)^*, \quad (12)$$

where $\mathbb{E}[\iota]$ denotes the mean of μ_0 , defined as:

$$\mathbb{E}[\iota] = \int_{L^2(\Omega)} \iota(q) d\mu_0(q), \quad \text{for every } \iota \in L^2(\Omega)^*. \quad (13)$$

Next we interpret (12) in a more intuitive manner and express the covariance operator differently. According to the Hahn-Banach theorem, we know that $\iota(q)$ serves, to some extent, as a means of extracting the coordinate of q . This implies that $C_0(\iota_1, \iota_2)$ represents the covariance between different coordinates, ι_1, ι_2 , of q . By the Riesz representation theorem, we no longer distinguish between $L^2(\Omega)$ and its dual $L^2(\Omega)^*$ in the following. Let $\{\varphi_n\}_{n=1}^\infty$ be an orthonormal basis of $L^2(\Omega)$. The Fourier expansion of q is given by $q(x) = \sum_{n=1}^\infty q_n \varphi_n(x)$. As taking ι as φ_i, φ_j , it gets the coordinates q_i, q_j of q by $\iota(q)$. It can be seen that the mean and covariance operators are bounded linear and bilinear functional respectively. The bounded bilinear functional determines a bounded linear operator as follows:

$$C_0(\iota_1, \iota_2) = \langle C_0 \iota_1, \iota_2 \rangle, \quad (14)$$

where the same notation is used for both the bilinear functional and the operator. In the present paper, we consider two commonly used forms of C_0 . The first is to define the covariance operator C_0 as an integral operator with a mean squared exponential kernel:

$$C_0^{\text{exp}} \iota = \int_{\Omega} \exp\left(-\frac{|x-y|^2}{2l^2}\right) \iota(y) dy, \quad (15)$$

where $l > 0$ is a length-scale parameter. We usually use the period version of C_0^{exp} in some case of periodic structure, i.e., the periodic mean squared exponential kernel covariance operator C_0^{per}

$$C_0^{\text{per}} \iota = \int_{\Omega} \exp\left(-\frac{2 \sin^2(\pi|x-y|/p)}{l^2}\right) \iota(y) dy, \quad (16)$$

where $l > 0$ is a length-scale parameter and $p > 0$ is a periodicity parameter. The second is to define $C_0^{-\Delta} = (-\Delta)^{-s}$ with Dirichlet boundary conditions. Note that C_0 is symmetric positive and of trace class. The range of $C_0^{\frac{1}{2}}$

$$E = \left\{ q = C_0^{\frac{1}{2}} w \mid w \in L^2(\Omega) \right\} \subset L^2(\Omega),$$

which is a Hilbert space equipped with inner product [36]

$$\langle \cdot, \cdot \rangle_E = \langle C_0^{-\frac{1}{2}} \cdot, C_0^{-\frac{1}{2}} \cdot \rangle_{L^2(\Omega)},$$

is called the Cameron-Martin space of measure μ_0 .

In this paper, our goal is to estimate the unknown $q \in K$ from measured data u^η . The exact u is related to q via the forward model (1) and the data u^η is collected by (3). For convenient, we assume that the data is collected at some discrete points uniformly distributed in the domain Ω and denote the forward model as

$$u^\eta(x_i) = G(q)(x_i) + \eta(x_i), \quad x_i \in \Omega, \quad i = 1, 2, \dots, m, \quad (17)$$

where $G : K \rightarrow \mathbb{R}^m$ and η is an m -dimensional zero mean Gaussian noise with covariance matrix Σ . Under this assumption, we have the likelihood function, i.e., the distribution of u^η conditional on q is

$$\pi(u^\eta|q) \propto \exp(-\Phi(q; u^\eta)), \quad (18)$$

where

$$\Phi(q; u^\eta) := \frac{1}{2} \|G(q) - u^\eta\|_\Sigma^2 = \frac{1}{2} \|\Sigma^{-1/2} (G(q) - u^\eta)\|_2^2, \quad (19)$$

is often referred to as the data fidelity term in deterministic inverse problems. The Bayesian approach provides decision making under uncertainty, while the prior distribution gives additional information about uncertainty. Here we assume that the prior measure of q is μ_{pr} , and the posterior measure μ_{post} is given by the Radon-Nikodym derivative:

$$\frac{d\mu_{\text{post}}}{d\mu_{\text{pr}}}(q) = \frac{1}{Z} \exp(-\Phi(q; u^\eta)), \quad (20)$$

where Z is a normalization constant. The most widely used prior in Bayesian inverse problems is the Gaussian prior, i.e., $\mu_{\text{pr}} = \mu_0$, where $\mu_0 = N(0, C_0)$. In practical terms, this Gaussian prior reflects a belief that the unknown parameter q has zero mean and that the covariance C_0 encodes our assumptions about the spread or uncertainty in q .

The concept of hybrid priors originates from the work of Z. Yao et al. [42]. Their approach introduces a more flexible prior that leverages the strengths of both probabilistic and total variation methods, aiming to enhance modeling in complex systems where both uncertainty and structure play critical roles. We present a new hybrid prior that combines the strengths of Gaussian distributions with topological information. This approach aims to incorporate the uncertainty modeling of Gaussian priors with a structured topological perspective, allowing for more nuanced and informative priors in settings where the underlying structure plays a crucial role. The Gaussian component provides a probabilistic framework with a known covariance structure, while the topological information offers insights into the shape, connectivity, or features of the underlying parameter space. By blending these two, we can achieve a prior that reflects both the variability in the data and the inherent structural constraints of the system.

In [42], rather than simply setting $\mu_{\text{pr}} = \mu_0$, the prior measure is defined as

$$\frac{d\mu_{\text{pr}}}{d\mu_0}(q) \propto \exp(-R(q)),$$

where $R(q)$ incorporates additional information beyond the Gaussian prior. Under this assumption, it immediately follows that the Radon-Nikodym derivative of μ_{post} with respect to μ_0 is given by

$$\frac{d\mu_{\text{post}}}{d\mu_0}(q) \propto \exp(-\Phi(q; u^\eta) - R(q)),$$

which recovers the standard formulation with Gaussian priors.

In [42], Yao et al. considered the case where the sample space is the Sobolev space $H^1(\Omega)$, defined as follows:

$$H^1(\Omega) = \{q \in L^2(\Omega) \mid \partial_x^\alpha q \in L^2(\Omega) \text{ for all } |\alpha| \leq 1\},$$

where $\alpha = (\alpha_1, \alpha_2, \dots, \alpha_s)$ and $|\alpha| = \sum_{i=1}^s \alpha_i$, and the associated norm is

$$\|q\|_{H^1} = \sum_{|\alpha| \leq 1} \|\partial_x^\alpha q\|_{L^2(\Omega)}.$$

The regularization term is chosen to be the TV seminorm [42]

$$R(q) = \lambda \|q\|_{\text{TV}} = \lambda \int_{\Omega} \|\nabla q\|_2 dx, \quad (21)$$

where λ is a prescribed positive constant.

We present a novel prior term grounded in the concept of persistence distance, as introduced through persistence pairs in [43]. To interpret the relative conceptions, we consider the triangulation of the graph of the unknown function q . This triangulation forms a simplicial complex (denoted by Q) that is homeomorphic to the graph of q . We also interpret the triangulation as a linear spline approximation of q on some partition I with knots $\{x_i\}_{i=0}^m$. The simplicial complex Q , together with the lower star filtration of Q , is denoted as \mathcal{Q} .

3.1 1-d case

First, we consider the case of 1-dimensional function. We denote the spline approximation by q , i.e., q is a piecewise linear function with $q(x_i) = q(x_i)$ and denote the space of linear splines with the partition I by $S_1(I)$. We need to introduce the concept of persistence distance based on persistence pairs and the corresponding difference of function values of q . The persistence distance consists of a sum of distances of function values of q being local extrema of the function q . It can be proven that the persistence distance is closely related to the discrete total variation of q . Compared to the discrete total variation, the persistence distance contains more information about the topological structure of the function [43]. For clarification, we first define the (one-sided) local maxima and minima of q introduced in [43].

Definition 3.1. [43] *A knot $x_l \in I \setminus \{x_0, x_m\}$ is called (left-sided) local minimum knot of $\mathbf{y} = (q(x_j))_{j=0}^m$ on I with the local minimum value $y_l = q(x_l)$, if $y_{l-1} = q(x_{l-1}) > q(x_l)$, and if there exists a $\nu \in \mathbb{N}_0$ such that $l + \nu + 1 \leq m$ and*

$$q(x_l) = q(x_{l+1}) = \dots = q(x_{l+\nu}) < q(x_{l+\nu+1}).$$

Analogously, a knot $x_l \in I \setminus \{x_0, x_m\}$ is called (left-sided) local maximum knot of $\mathbf{y} = (q(x_j))_{j=0}^m$ on I with the local maximum value $y_l = q(x_l)$, if $y_{l-1} = q(x_{l-1}) < q(x_l)$, and if there exists a $\nu \in \mathbb{N}_0$ such that $l + \nu + 1 \leq m$ and

$$q(x_l) = q(x_{l+1}) = \dots = q(x_{l+\nu}) > q(x_{l+\nu+1}).$$

The boundary knot $x_0 \in I$ is called (left-sided) local minimum (resp. maximum) knot of $\mathbf{y} = (q(x_j))_{j=0}^m$ on I with the local maximum value $y_0 = q(x_0)$, if there exists a $\nu \in \mathbb{N}_0$ with $\nu \leq m - 1$ such that

$$q(x_0) = q(x_1) = \dots = q(x_\nu) < q(x_{\nu+1}).$$

(resp. $q(x_0) = q(x_1) = \dots = q(x_\nu) > q(x_{\nu+1})$). The boundary knot $x_m \in I$ is called local minimum (resp. maximum) knot of $\mathbf{y} = (q(x_j))_{j=0}^m$ on I with the local minimum (resp. maximum) value $y_m = q(x_m)$, if $q(x_{m-1}) > q(x_m)$ (resp. $q(x_{m-1}) < q(x_m)$) holds.

Now we denote the subsets of $\{y_j : j = 0, \dots, m\}$,

$$\begin{aligned} Y_m &:= \{y_k = q(x_k) : y_k \text{ is a local minimum value of } \mathbf{y}\}, \\ Y^m &:= \{y_k = q(x_k) : y_k \text{ is a local maximum value of } \mathbf{y}\}, \end{aligned}$$

as well as the corresponding subsets of the partition I ,

$$\begin{aligned} I_m &:= \{x_k : q(x_k) \in Y_m\}, \\ I^m &:= \{x_k : q(x_k) \in Y^m\}. \end{aligned}$$

Let $I_{\max} := \max\{I_m, I^m\}$ denote the extremum knot with the highest index in the set $I_m \cup I^m$. Note that I_{\max} may not necessarily coincide with x_m , as there could exist some $\nu < m$ for which $q(x_\nu) = \dots = q(x_{m-1}) = q(x_m)$. Let $\#Y$ represent the number of elements in a set Y . It is straightforward to observe that, after ordering the knots $x_k \in I_m \cup I^m$ by their values, each local minimum (maximum) knot is always adjacent to a local maximum (minimum) knot. Consequently, the relationship

$$\#Y_m - \#Y^m \in \{-1, 0, 1\}$$

holds.

Definition 3.2. [43] *The knot $x_l \in I_m$ is called global minimum knot of $y = (q(x_j))_{j=0}^m$ on I with the global minimum value $q(x_l)$ if $x_l = \arg \min_{x \in I_m} q(x)$. The knot $x_l \in I_m$ is called global maximum knot of $y = (q(x_j))_{j=0}^m$ on I with the global maximum value $q(x_l)$ if $x_l = \arg \max_{x \in I_m} q(x)$.*

If the global maximum (or minimum) knot is not uniquely determined according to Definition 3.2, we select the knot x_l with the smallest index l . This method accounts for the scenario where the function achieves its global maximum or minimum at multiple knots, ensuring a consistent and unambiguous choice.

As discussed in [43], applying Algorithm 1 in practical scenarios is challenging. Drawing on the concept of persistence in Morse functions [14], a new pairing procedure for a one-dimensional function is proposed in [43]. This algorithm examines the local maxima and minima of the function and pairs them according to the idea that a (local) minimum at x creates and represents a new component of the level set $\mathbb{R}_x = q^{-1}((-\infty, x])$. At a (local) maximum, two components of the level set merge, and we pair the maximum with the higher representative of these two components. The resulting merged component is then represented by the lower minimum. An equivalent description is as follows: when passing a maximum, we pair it with the higher neighboring minimum and remove the paired values from the set of local extrema (see [14]). The following algorithm list the persistence pairing procedure as in [43], which construct persistence pairs (x_k, x_l) of $\mathbf{y} = (q(x_j))_{j=0}^m$ over the partition I .

Algorithm 2 provides at least $\#Y^m - 2$ persistence pairs, as each local maximum knot of q (or y) that is not on the boundary (i.e., not in $\{x_0, x_{\max}\}$) is paired with a local minimum knot. Additionally, each local minimum knot that is not the global minimum knot is included in exactly one persistence pair, while the global minimum knot remains unpaired. A boundary knot (i.e., x_0 or x_{\max}) appears in a persistence pair if it is a local but not the global minimum knot; however, it is not included in any persistence pair if it is a local maximum knot or the global minimum knot.

Algorithm 2

- 1: **Input:** Y_m, Y^m, I_m, Y^m for $\mathbf{y} = (q(x_j))_{j=0}^m$.
 - 2: Let $r := \#Y^m$, $P_1 = \emptyset$ and $I_{m,0} := I_m$. Fix the ordered set $K_0 = \{q(x_{k_1}) \leq \dots \leq q(x_{k_r})\}$ of all local maximum values in Y^m using the convention that for $q(x_k) = q(x_l) \in Y^m$, we take $q(x_k)$ first if $x_k < x_l$.
 - 3: **for** $l = 1, \dots, r$ **do**
 - Consider the l -th entry $q(x_{k_l})$ in the ordered set K_0 .
 - If $x_{k_l} \notin \{x_0, x_{\max}\}$ then find the two spatial neighbors $\tilde{x}_1, \tilde{x}_2 \in I_{m,l-1}$ of x_{k_l} .
 - Put $\tilde{x} := \arg \min_{x \in \{\tilde{x}_1, \tilde{x}_2\}} |q(x_{k_l}) - q(x)|$, where in case of $|q(x_{k_l}) - q(\tilde{x}_1)| = |q(x_{k_l}) - q(\tilde{x}_2)|$ we take $\tilde{x} = \max\{\tilde{x}_1, \tilde{x}_2\}$.
 - Then (\tilde{x}, x_{k_l}) resp. (x_{k_l}, \tilde{x}) is a persistence pair of q , and we set $P_1 = P_1 \cup \{(\tilde{x}, x_{k_l})\}$ and $I_{m,l} := I_{m,l-1} \setminus \{\tilde{x}\}$.
 - Here we apply the convention that the knots in the persistence pairs are ordered by size, i.e., we write (\tilde{x}, x_{k_l}) if $\tilde{x} < x_{k_l}$ and (x_{k_l}, \tilde{x}) if $\tilde{x} > x_{k_l}$.
 - 4: **end for**
 - 5: **Output:** P_1 containing all persistence pairs of \mathbf{y} (resp. q).
-

In computational topology, barcodes and persistence diagrams are the popular visualization tools to display the persistence pairs. Each persistence pair (x_k, x_l) corresponds to the point $(q(x_k), q(x_l))$ in the persistence diagram, and the distance of this point to the diagonal line $y = x$, given by $|q(x_k) - q(x_l)|$, reflects the “topological significance” of the pair, which gives us some information about the “topological relevance” of these two local extrema of q . Important features correspond to points being further away from the diagonal, i.e., to persistence pairs (x_k, x_l) with significant distances $|q(x_k) - q(x_l)|$. And the boundary extremum knots x_0 and x_{\max} are contained in at most one persistence pair, either in one from P_1 or in one from P_2 , since they are not regarded when being a local maximum knot. Indeed, x_0 (resp. x_{\max}) will not occur in any persistence pair, i.e., neither in P_1 nor in P_2 , if it is a global extremum knot.

Definition 3.3. [43] For a given piecewise linear spline function $q \in S_1(I)$ respective the vector $\mathbf{y} = (q(x_j))_{x_j \in I}$, we define the persistence distance by

$$\|q\|_{\text{per}} = \|\mathbf{y}\|_{\text{per}} = \|\mathbf{y}|I\|_{\text{per}} := \sum_{(x_k, x_l) \in P_1} |q(x_l) - q(x_k)| + \sum_{(x_k, x_l) \in P_2} |q(x_l) - q(x_k)|,$$

i.e., as the sum over all distances of function values for the persistence pairs in P_1 and P_2 .

When applying Algorithm 2 to the sequence $\{-q(x_j)\}_{j=0}^m$, we can obtain a second set P_2 of persistence pairs for q (resp. for \mathbf{y}) on I . It can be seen that P_1 and P_2 partially coincide, but usually are not equal. When persistence pairs occur twice, i.e., when they are included in $P_1 \cup P_2$, the corresponding absolute differences of function values are counted twice. A set in which an element can appear multiple times is referred to as a multiset. We list some properties of the persistence distance $\|q\|_{\text{per}} = \|\mathbf{y}\|_{\text{per}}$ given in [43].

Theorem 3.1. [43] Let $q \in S_1(I)$ be a spline function with $\mathbf{y} = (q(x_j))_{j=0}^m$ on the partition $I = \{x_0, \dots, x_m\}$ of Ω . Then the persistence distance $\|q\|_{\text{per}} = \|\mathbf{y}\|_{\text{per}} = \|\mathbf{y}|I\|_{\text{per}}$ satisfies the following properties.

- (1) $\|\mathbf{y}\|_{\text{per}} \geq 0$. We have $\|\mathbf{y}\|_{\text{per}} = 0$ if and only if $\mathbf{y} = (y_j)_{j=0}^m$ is monotone.
- (2) For each $c \in \mathbb{R}$, we have $\|c\mathbf{y}\|_{\text{per}} = |c| \cdot \|\mathbf{y}\|_{\text{per}}$.
- (3) The persistence distance is invariant under addition of a constant function,

$$\|\mathbf{y} + c\mathbf{1}\|_{\text{per}} = \|\mathbf{y}\|_{\text{per}},$$

where $\mathbf{1} = (1, \dots, 1)^T \in \mathbb{R}^{m+1}$ and $c \in \mathbb{R}$. In particular, $\|c\mathbf{1}\|_{\text{per}} = 0$.

- (4) The persistence distance $\|\mathbf{y}\|_{\text{per}} : \mathbb{R}^{m+1} \rightarrow \mathbb{R}$ is a continuous functional.
- (5) The persistence distance $\|\mathbf{y}\|_{\text{per}}$ is submodular, i.e., for $\mathbf{p}, \mathbf{q} \in S_1(I)$ with $\mathbf{y} = (\mathbf{p}(x_j))_{j=0}^m$ and $\mathbf{z} = (\mathbf{q}(x_j))_{j=0}^m$ we have

$$\|\mathbf{y}\|_{\text{per}} + \|\mathbf{z}\|_{\text{per}} \geq \|\max(\mathbf{y}, \mathbf{z})\|_{\text{per}} + \|\min(\mathbf{y}, \mathbf{z})\|_{\text{per}},$$

where $\max(\mathbf{y}, \mathbf{z}) := (\max\{y_j, z_j\})_{j=0}^m$ and $\min(\mathbf{y}, \mathbf{z}) := (\min\{y_j, z_j\})_{j=0}^m$.

- (6) There exist $\mathbf{y}, \mathbf{z} \in \mathbb{R}^{m+1}$ such that the persistence distance $\|\cdot\|_{\text{per}}$ does not satisfy the triangle inequality, i.e.,

$$\|\mathbf{y} + \mathbf{z}\|_{\text{per}} \leq \|\mathbf{y}\|_{\text{per}} + \|\mathbf{z}\|_{\text{per}}.$$

Hence $\|\cdot\|_{\text{per}}$ is not convex.

While being not a semi-norm, the persistence distance conveys substantial information about the structure of a function $q \in S_1(I)$ and is closely related to the discrete total variation $\text{TV}(q)$. It can be proven that the following theorem holds [43].

Theorem 3.2. [43] Let I be a partition of Ω . Then for each function $q \in S_1(I)$, we have

$$\|q\|_{\text{per}} + \max_{x, \tilde{x} \in I} |q(x) - q(\tilde{x})| = \text{TV}(q),$$

where $\text{TV}(q)$ is the discrete total variation of q defined by

$$\text{TV}(q) := \sum_{j=0}^{m-1} |q(x_{j+1}) - q(x_j)|.$$

In contrast to the total variation $\text{TV}(q)$, the persistence distance is a sum of the differences in function values at the local extrema of q , reflecting the topological properties of the function. Small distances $|q(x) - q(\tilde{x})|$, corresponding to closely paired extrema (x, \tilde{x}) , are associated with oscillatory behavior such as noise. In contrast, large distances $|q(x) - q(\tilde{x})|$ represent significant features of the function q . Let for simplicity

$$P(q) = P_1 \cup P_2 \cup \{(x, \tilde{x})\}$$

be the set of all (persistence) pairs, where (x, \tilde{x}) denotes the pair of knots whose corresponding function values are the global minimum and the global maximum of q . For the one-dimensional case, we define the prior as

$$\frac{d\mu_{\text{pr}}}{d\mu_0}(q) \propto \exp \left(- \sum_{(x_j, \tilde{x}_j) \in P(q)} \alpha_j(q) |q(x_j) - q(\tilde{x}_j)| \right), \quad (22)$$

where $\alpha_j = \alpha_j(\mathbf{q}) = \alpha(\mathbf{q}, x_j, \tilde{x}_j)$ depends on the persistence $|\mathbf{q}(x_j) - \mathbf{q}(\tilde{x}_j)|$. This corresponds to taking the regularization term $R_{1d}(\mathbf{q})$ as

$$R_{1d}(\mathbf{q}) = \sum_{(x_j, \tilde{x}_j) \in P(\mathbf{q})} \alpha_j(\mathbf{q}) |\mathbf{q}(x_j) - \mathbf{q}(\tilde{x}_j)|. \quad (23)$$

The parameter α should be large for small distances $|\mathbf{q}(x_j) - \mathbf{q}(\tilde{x}_j)|$, emphasizing the penalization of minor oscillations or noise. Conversely, α should be relatively small for large distances $|\mathbf{q}(x_j) - \mathbf{q}(\tilde{x}_j)|$, allowing significant features of the function \mathbf{q} to be preserved. In [43], the weight strategy is proposed to deal with denoising problems

$$\alpha_j(\mathbf{q}) = (\kappa_j + 1)\theta \frac{1}{1 + \beta |\mathbf{q}(\tilde{x}_j) - \mathbf{q}(x_j)|}, \quad (24)$$

where $\beta > 0$ and $\kappa_j = \kappa(x_j, \tilde{x}_j)$ is the order of the pair (x_j, \tilde{x}_j) in its chain of pairs and $\theta > 1$.

3.2 2-d case

The concept of the 1-dimensional persistence prior can be extended to the 2-dimensional case. We only consider the case where Ω is a square domain. In this case, q can be viewed as an image. The values of q on vertices of the triangulation are arranged in a matrix. We denote this matrix as $\mathbf{Q} = [Q_{ij}]$, $i = 1, \dots, I$, $j = 1, \dots, J$, the i -th row as \mathbf{Q}^i , and the j -th column as \mathbf{Q}_j . The rows and columns of \mathbf{Q} are then processed in a manner similar to the 1-dimensional case. We treat each row (resp. column) as a vertex set of some 1-d spline function. To simplify the notation, we use q^i and q_j to denote the linear spline function with knot values \mathbf{Q}^i and \mathbf{Q}_j respectively. Then we impose a topological-Gaussian prior on each row (resp. column) and sum them, i.e., we take

$$R_{2d}(q) = \sum_{i=1}^I R_{1d}(q^i) + \sum_{j=1}^J R_{1d}(q_j), \quad (25)$$

and set

$$\frac{d\mu_{\text{pr}}}{d\mu_0}(q) \propto \exp(-R_{2d}(q)). \quad (26)$$

In [37], A. Stuart proved that the posterior μ_{post} is a well-defined probability measure on a separable Banach space S and that it is Lipschitz continuous, for example, in the sense of the Hellinger metric, with respect to the data u if the forward map G satisfies certain conditions. Z. Yao et al. [42] analyzed the well-posedness under a slightly different assumption using the hybrid prior. J. Latz provided more relaxed assumptions to further investigate the well-posedness of the posterior distribution [32, 33]. From the analysis in [32, 33], it can be seen that Bayesian inverse problems are generally well-posed.

4 Numerical tests

In this section, we give some numerical examples to verify the effectiveness of the proposed prior. We test the Gaussian priors, TV-Gaussian prior and the proposed TP-Gaussian

prior and compare the numerical effectiveness. In all numerical tests, the data is generated by adding a 1‰ relative error to the numerical solution using the exact q , i.e.,

$$u^n(x) = u(q)(x) + \eta(x), \quad \eta = 1\text{‰}\|u(q)\|\xi, \quad (27)$$

where $u(q)$ is the numerical solution and $\xi \sim N(0, I)$. We apply Metropolis-Hastings algorithm (see Algorithm 3) to generate some posterior samples from the posterior distribution [42]. When using this algorithm, it is necessary to incorporate a burn-in phase and apply lag to ensure that the samples are drawn from the stationary distribution, reducing the impact of initial transients and minimizing autocorrelation between consecutive samples. In our numerical tests, we uniformly discard the first half of the samples as the burn-in period and set the lag to 5. The sample mean is used to the estimation of q .

Algorithm 3

- 1: **Initialization:** Set sample number N and $q^{(0)} = 0$. Compute the corresponding negative log likelihood function $\Phi(q^{(0)}; u^n)$ and regularization term $R(q^{(0)})$. Denote

$$\varphi^{(0)} := \Phi(q^{(0)}; u^n) + R(q^{(0)}).$$

- 2: Move the sample to a proposal $\hat{q}^{(n)} = \sqrt{1 - \rho^2}q^{(n-1)} + \rho\xi$, where $\xi \sim \mu_0$.
- 3: Compute the negative log likelihood function $\Phi(\hat{q}^{(n)}; u^n)$ and regularization term $R(\hat{q}^{(n)})$. Denote

$$\hat{\varphi}^{(n)} := \Phi(\hat{q}^{(n)}; u^n) + R(\hat{q}^{(n)}).$$

- 4: Compute the accept probability $\alpha = \min\{1, \exp[\hat{\varphi}^{(n)} - \varphi^{(n-1)}]\}$.
 - 5: Set $q^{(n)} = \hat{q}^{(n)}$ if $\alpha > r$, else $q^{(n)} = q^{(n-1)}$, where r is a uniform random number on $[0, 1]$.
 - 6: When $n < N$, implement step 2 - step 5.
-

Example 0. First, we consider a smooth 1-dimensional function in $\Omega = (0, 1)$

$$q(x) = 1 + x(1 - x) \sin(4\pi x).$$

We generate $N = 10^5$ samples according to Algorithm 3. In this test, we compare the effectiveness of different priors presented in Section 3, namely the Gaussian prior with $C_0^{-\Delta}$ (with $s = 1.5$) and the periodic mean exponential kernel C_0^{per} , the TV-Gaussian prior, and the TP-Gaussian prior. For the latter two cases, we use the periodic mean squared exponential kernel Gaussian in μ_0 . The parameters in these priors are set to $l = 1.0$, $p = 1$ in C_0^{per} , $\theta = 3$ and $\beta = 0.001$ in (24) of the topological prior. The weight parameter λ in the TV-Gaussian prior, and the TP-Gaussian prior is set to 4. The proposal parameter ρ in Algorithm 3 is set to 0.002. The numerical reconstructions are presented in Fig. 3, demonstrating that the proposed prior is well-suited for the smooth scenario. From the displayed results, it is evident that the TP-Gaussian prior is competitive with the other priors.

Example 1. In the second example, we consider the exact q as a 1-dimensional piecewise constant function on $\Omega = (0, 1)$:

$$q(x) = \begin{cases} 1.5, & \frac{1}{3} \leq x < \frac{2}{3}, \\ 0.5, & \text{otherwise.} \end{cases}$$

This numerical experiment demonstrates the performance of both the baseline prior from Example 0 and the proposed prior μ_0 with the kernel $C_0^{-\Delta}$ (with parameter $s = 1.6$). For consistency with Example 0, we explicitly list only the modified parameters: the length scale $l = 0.2$ in C_0^{per} , the regularization weight $\lambda = 20$, and the proposal step size $\rho = 0.01$. The numerical comparison is given in Fig. 3. Obviously, when dealing with a function that has jumps, using only a Gaussian prior leads to unsatisfactory results. Specifically, the Gaussian prior μ_0 with $C_0^{-\Delta}$ enforces an excessively high degree of smoothness on the function due to its highly smooth eigenfunctions within the domain. This makes it difficult to capture local features, especially for non-smooth functions. Whether using the Karhunen-Loève expansion, finite difference methods, or finite element methods to discretize the covariance operator $C_0^{-\Delta}$, we encounter the problem that either the number of expansion terms becomes too large, or the discretization grid is limited by machine precision, preventing the capture of local features. When using μ_0 with C_0^{per} , the result exhibits oscillations, likely arising from the properties of the periodic exponential covariance kernel, particularly its inherent smoothness and long-range dependencies, which can introduce oscillatory artifacts into the solution. In contrast, the TV-Gaussian and TP-Gaussian priors can significantly alleviate these issues. In the subsequent examples, we will no longer employ μ_0 with the covariance operator $C_0^{-\Delta}$, as our focus is solely on testing non-smooth scenarios.

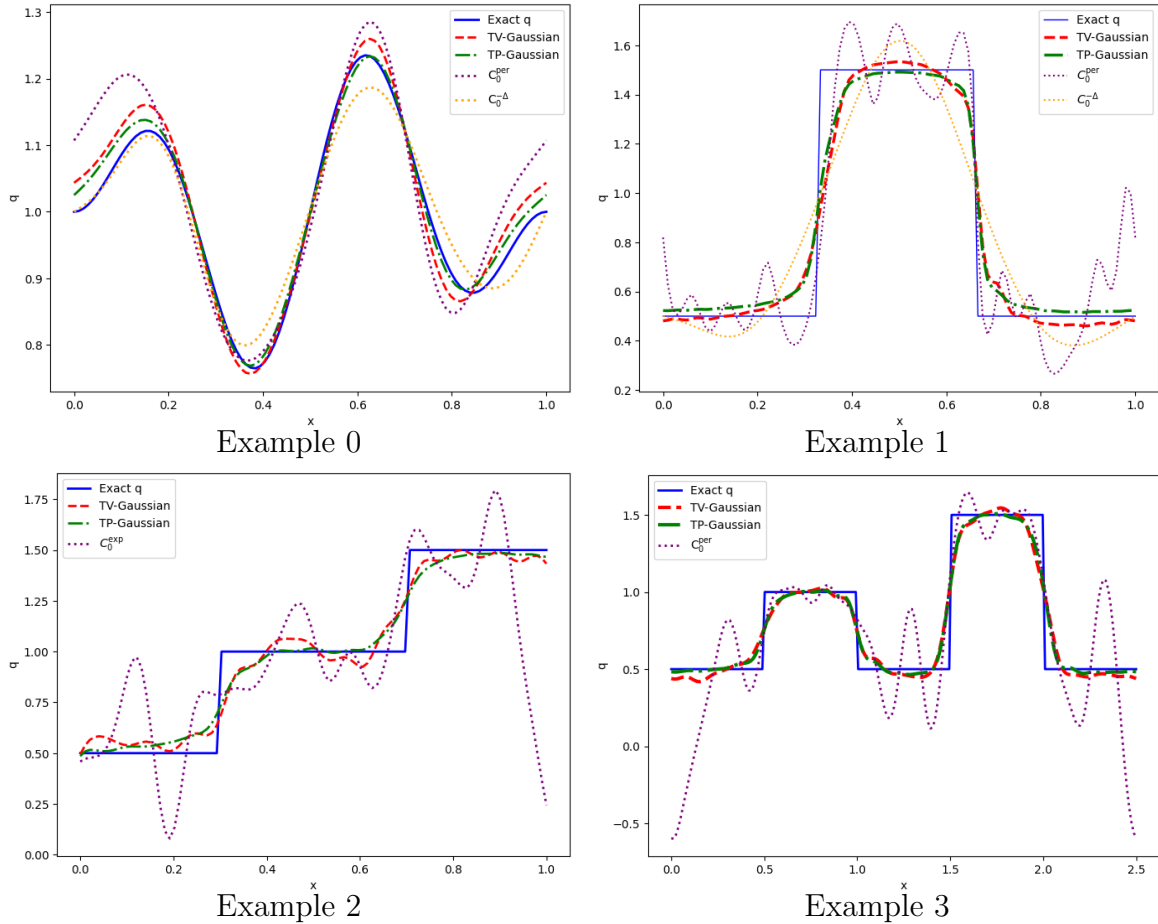


Figure 3: Numerical comparisons using different priors for 1d case.

Example 2. We test the proposed prior on a 1D step function,

$$q(x) = \begin{cases} 0.5, & 0 \leq x < 0.3, \\ 1, & 0.3 \leq x < 0.7, \\ 1.5, & 0.7 \leq x \leq 1. \end{cases}$$

In this example, the Gaussian measure μ_0 with C_0^{exp} is used as the base measure in the Gaussian, TV-Gaussian, and TP-Gaussian priors. The parameter l is set to 0.05 in all cases. The weight parameter λ is set to 10, and the Markov transition parameter β is set to 0.005. Other parameters are chosen to be the same as in Example 1. The numerical results are displayed in Fig. 3. As in Example 1, the oscillation occurs when using the prior μ_0 with the exponential covariance kernel and the reason is similar to that in Example 1. In addition, the TV-Gaussian and TP-Gaussian priors can fulfill the case well.

Example 3. As in Example 1, we adjust the piecewise constant to a more complicated case as

$$q(x) = \begin{cases} 0.5, & 0 \leq x < 0.5, \\ 1, & 0.5 \leq x < 1.0, \\ 0.5, & 1.0 \leq x \leq 1.5, \\ 1.5, & 1.5 \leq x < 2.0, \\ 0.5, & 2.0 \leq x \leq 2.5. \end{cases}$$

We still use the periodic mean squared exponential kernel Gauss as the base measure with $l = 0.2$, $p = 2.5$. The weight parameter $\lambda = 20$. The parameter of the topological prior $\theta = 3$ and $\beta = 0.001$ in (24). We generate 2×10^5 samples by Algorithm 3. From the displayed results (see Fig. 3), it is evident that the same phenomenon observed in Examples 1 and 2 is replicated here.

Example 4. In this example, we consider a function that is derived from the Weierstrass function

$$W(x) = \sum_{n=0}^{\infty} a^n \cos(b^n \pi x),$$

where $0 < a < 1$, b is a positive odd integer and $ab > 1 + \frac{3\pi}{2}$. By $W_K(x)$ we denote the truncated series to the first $K + 1$ terms. Take the exact q as $q(x) = \frac{2}{\pi} \arctan(W_K(x)) + 1$ with $a = 0.4$, $b = 4$ and $K = 10$. Here, we do not adhere to the strict parameter rule in the Weierstrass function. In the sampling process, we apply a transform $q(x) = \exp(g(x))$ and treat g as the unknown target. As in example 2, the mean squared exponential kernel Gaussian is used as the base measure. We set $l = 0.01$ and the weight parameter $\lambda = 5$. This test reveals that the oscillatory limitations of the squared exponential kernel prior are exacerbated, whereas our approach still achieves robust performance (see Fig. 4). It should be noted that we cannot assert the numerical performance of the TP-Gaussian prior is superior to that of the TV-Gaussian prior based solely on this example. The differences observed in Fig. 4 are partly influenced by the parameter settings, particularly the weight parameter λ . However, when the weight parameter λ is held constant, the TP-Gaussian prior yields more robust results compared to the TV-Gaussian prior. In the regularization framework, the weight parameter acts as the regularization parameter,

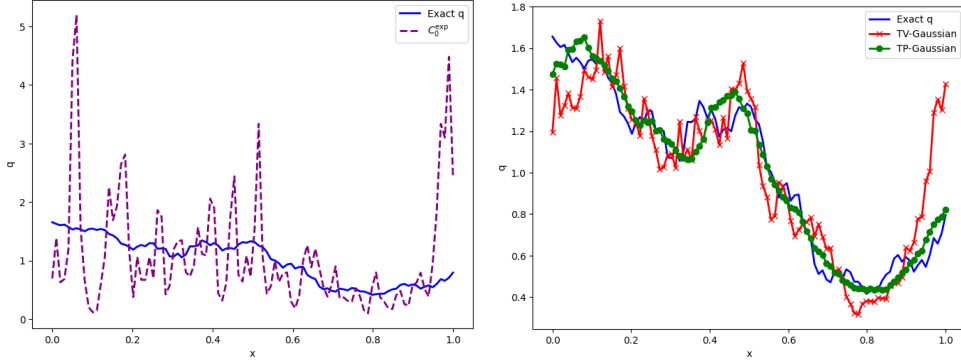


Figure 4: Numerical comparisons using different priors for Example 4.

which is both crucial and challenging to select. Consequently, the TP-Gaussian prior offers a more flexible and adaptable algorithm.

Example 5. We consider a 2d piecewise constant function in a squared domain $\Omega = (0, 1) \times (0, 1)$

$$q(x, y) = \begin{cases} 1.5, & (x - 0.5)^2 + (y - 0.5)^2 \leq 0.25^2, \\ 0.5, & \text{otherwise.} \end{cases}$$

In this example, we take $\mu_0 = N(0, C_0^{\text{exp}})$ with the parameter $l = 0.1$. We generate $N = 40,000$ samples. The weight parameter λ in the TV-Gaussian and TP-Gaussian priors is set to 2. Other parameters remain the same as those in Example 1.

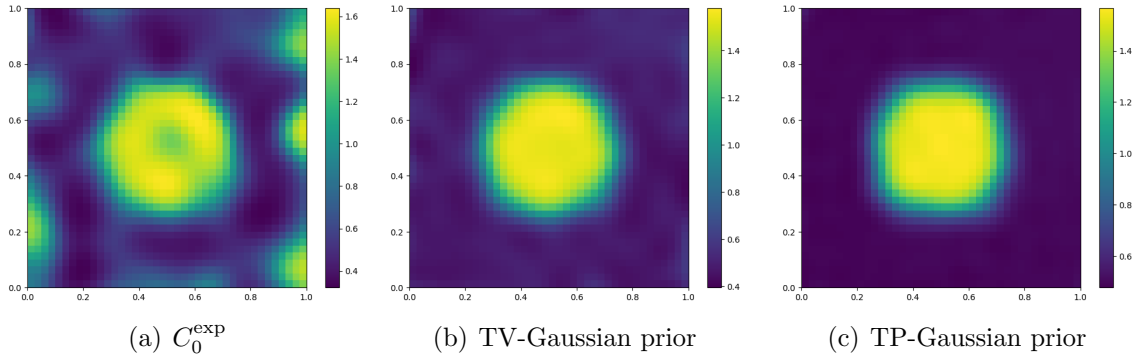


Figure 5: Numerical illustration using different priors for Example 5: (a) the Gaussian prior with C_0^{exp} ; (b) the TV-Gaussian prior; (c) the TP-Gaussian prior.

Example 6. We consider a 2d piecewise constant function in a squared domain $\Omega = (0, 2) \times (0, 2)$

$$q(x, y) = \begin{cases} 1, & (x - 0.6)^2 + (y - 0.6)^2 \leq 0.3^2, \\ 1.5, & (x - 1.4)^2 + (y - 1.4)^2 \leq 0.3^2 \\ 0.5, & \text{otherwise.} \end{cases}$$

In this example, apart from adjusting the parameter l to 0.1 and λ to 5, all other parameters remain the same as in Example 5.

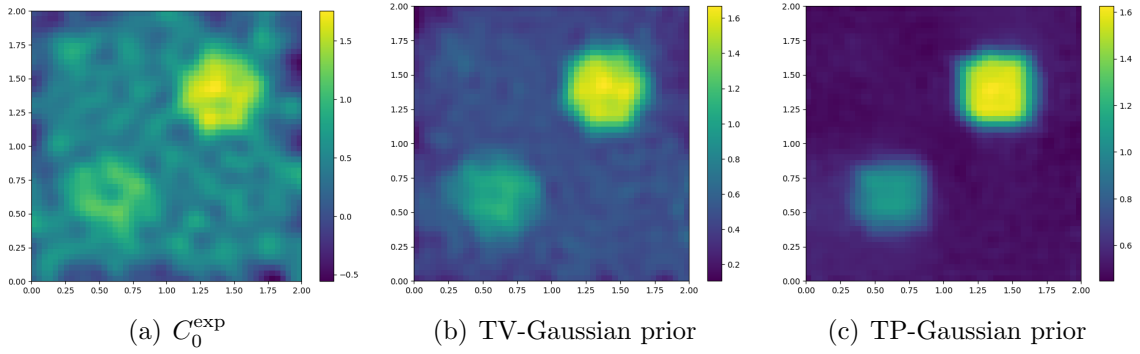


Figure 6: Numerical illustration using different priors for Example 6: (a) the Gaussian prior with C_0^{exp} ; (b) the TV-Gaussian prior; (c) the TP-Gaussian prior.

From the examples in the 2D case, we can draw conclusions that are nearly identical to those in the 1D case. This indicates that the TP-Gaussian prior produces reliable reconstruction results, which are competitive with those obtained using the TV-Gaussian prior and superior to the case where only the Gaussian prior is used.

5 Conclusion

We employ persistent homology as a tool to construct a hybrid prior for estimating the unknown variable in the inverse potential problem within the Bayesian framework. A key feature of this prior is that it constrains the topological variation of the unknown variable, effectively imposing a regularity condition akin to the total variation (TV). Moreover, the TP-based prior is defined on a topological space, which is a mild limitation. This flexibility allows the method to be easily extended to a broader range of applications. In numerical practice, the TP-Gaussian prior demonstrates excellent performance. Its ability to produce robust results is enhanced by the flexibility of its parameter settings, which allow for more adaptable and precise tuning.

References

- [1] G. Bal and G. Uhlmann. Inverse diffusion theory of photoacoustics. *Inverse Problems*, 26(085010):20pp, 2010.
- [2] J. M. Bardsley. Gaussian markov random field priors for inverse problems. *Inverse Problems and Imaging*, 7(2):397–416, 2013.
- [3] L. Baudouin and A. Mercado. An inverse problem for schrödinger equations with discontinuous main coefficient. *Applicable Analysis*, 87(10-11):1145–1165, 2008.
- [4] L. Baudouin and J. Puel. Uniqueness and stability in an inverse problem for the schrödinger equation. *Inverse Problems*, 18:1537–1554, 2002.
- [5] M. Benning and M. Burger. Modern regularization methods for inverse problems. *Acta Numerica*, pages 1–111, 2018.

- [6] A. Beskos, M. Girolami, S. Lan, P. Farrell, and A. Stuart. Geometric mcmc for infinite-dimensional inverse problems. *J. Comput. Phys*, 335:327–351, 2017.
- [7] Jean-Daniel Boissonnat, Frédéric Chazal, and Mariette Yvinec. *Geometric and Topological Inference*. Cambridge University Press, 2018.
- [8] T. Bui-Thanh and O. Ghattas. An analysis of infinite dimensional bayesian inverse shape acoustic scattering and its numerical approximation. *SIAM/ASA Journal on Uncertainty Quantification*, 2(1), 2014.
- [9] A. Carpio, S. Iakunin, and G. Stadler. Bayesian approach to inverse scattering with topological priors. *Inverse Problems*, 36(105001):29pp, 2020.
- [10] M. Choulli. Some stability inequalities for hybrid inverse problems. *Comptes Rendus. Mathématique*, 359(10):1251–1265, 2021.
- [11] M. Dashti and A. Stuart. *The Bayesian Approach to Inverse Problems*. Springer, 2017.
- [12] T. Dey and Y. Wang. *Computational Topology for Data Analysis*. Cambridge University Press, 2022.
- [13] N. Dunford and J. T. Schwartz. *Linear Operators, Part I: General Theory*, volume VII. John Wiley & Sons, 1988.
- [14] H. Edelsbrunner and J. Harer. Persistent homology—a survey. In J.E. Goodman, J. Pach, and R. Pollack, editors, *Surveys on Discrete and Computational Geometry: Twenty Years Later: AMS-IMS-SIAM Joint Summer Research Conference*, volume 453, pages 257–282. American Mathematical Society, 2008.
- [15] H. Edelsbrunner and J. Harer. *Computational Topology: An Introduction*. the American Mathematical Society, 2010.
- [16] H. Edelsbrunner, J. Harer, and A. Zomorodian. Hierarchical morse complexes for piecewise linear 2-manifolds. *Discrete Comput. Geom.*, (30):87–107, 2003.
- [17] H. Edelsbrunner, D. Letscher, and A. Zomorodian. Topological persistence and simplification. *Discrete Comput. Geom.*, 28:511–533, 2002.
- [18] H. Edelsbrunner, D. Morozov, and V. Pascucci. Persistence-sensitive simplification of functions on 2-manifolds. In *SCG '06 Proceedings of the Twenty-Second Annual Symposium on Computational Geometry*, pages 127–134, 2005.
- [19] H. W. Engl, K. Kunisch, and A. Neubauer. Convergence rates for tikhonov regularization of nonlinear ill-posed problems. *Inverse Problems*, 5:523–540, 1989.
- [20] H. W. Engl, K. Kunisch, and A. Neubauer. *Regularization of Inverse Problems*. Kluwer, 1996.
- [21] T. Furuya, P. Kow, and J. Wang. Consistency of the bayes method for the inverse scattering problem. *Inverse Problems*, 40(055001):24pp, 2024.
- [22] M. Giordano and R. Nickl. Consistency of bayesian inference with gaussian process priors in an elliptic inverse problem. *Inverse Problems*, 36(085001):35pp, 2020.

- [23] A. Hatcher. *Algebraic Topology*. Cornell Department of Mathematics, <http://www.math.cornell.edu/~hatcher>, 2001.
- [24] J. Huang, Z. Deng, and L. Xu. A bayesian level set method for an inverse medium scattering problem in acoustics. *Inverse Problems and Imaging*, 15(5):1077–1097, 2021.
- [25] M. A. Iglesias, K. Lin, and A. M. Stuart. Well-posed bayesian geometric inverse problems arising in subsurface flow. *Inverse Problems*, 30(114001):39pp, 2014.
- [26] M. A. Iglesias, Y. Lu, and A. M. Stuart. A bayesian level set method for geometric inverse problems. *Interface and Free Boundaries*, 18:181–217, 2016.
- [27] K. Ito and B. Jin. *Inverse Problems: Tikhonov Theory and Algorithms*. Hackensack, NJ: World Scientific, 2015.
- [28] B. Jin, X. Lu, Q. Quan, and Z. Zhou. Convergence rate analysis of galerkin approximation of inverse potential problem. *Inverse Problems*, 39(015008):26, 2023.
- [29] T. Kaczynski, K. Mischaikow, and M. Mrozek. *Computational Homology*. Springer-Verlag New York, 2004.
- [30] J. P. Kaipio, T. Huttunen, T. Luostari, T. Lähivaara, and P. B. Monk. A bayesian approach to improving the born approximation for inverse scattering with high-contrast materials. *Inverse Problems*, 35(084001):19pp, 2019.
- [31] J. P. Kaipio and E. Somersalo. *Statistical and Computational Inverse Problems*, volume 160. Springer, 1 edition, 2005.
- [32] J. Latz. On the well-posedness of bayesian inverse problems. *SIAM/ASA Journal on Uncertainty Quantification*, 8(1):451–482, 2020.
- [33] J. Latz. Bayesian inverse problems are usually well-posed. *SIAM Review*, 65(3):831–865, 2023.
- [34] Z. Li, Z. Deng, and J. Sun. Extended-sampling-bayesian method for limited aperture inverse scattering problems. *SIAM Journal on Imaging Sciences*, 13(1):422–444, 2020.
- [35] H. H. Pennes. Analysis of tissue and arterial blood temperatures in the resting human forearm. *J. Appl. Physiol.*, 1:93–122, 1948.
- [36] G. Da Prato. *An Introduction to Infinite-Dimensional Analysis*. Berlin: Springer, 2006.
- [37] A. M. Stuart. Inverse problems: A bayesian perspective. *Acta Numerica*, 19:451–559, 2010.
- [38] J. Tarantola. *Inverse Problem Theory and Methods for Model Parameter Estimation*. SIAM, 2005.
- [39] D. Trucu, D. B. Ingham, and D. Lesnic. Space-dependent perfusion coefficient identification in the transient bio-heat equation. *J. Engrg. Math.*, 67:307–315, 2010.

- [40] Z. Wang, J. M. Bardsley, A. Solonen, T. Cui, and Y. M. Marzouk. Bayesian inverse problems with l_1 priors: A randomize-then-optimize approach. *SIAM Journal on Scientific Computing*, 39(5), 2017.
- [41] M. Yamamoto and J. Zou. Simultaneous reconstruction of the initial temperature and heat radiative coefficient. *Inverse Problems*, 17:1181–1202, 2001.
- [42] Z. Yao, Z. Hu, and J. Li. A tv-gaussian prior for infinite-dimensional bayesian inverse problems and its numerical implementations. *Inverse Problems*, 32(7):075006, 2016.
- [43] Y. Zheng. *Application of Persistent Homology in Signal and Image Denoising*. PhD thesis, Georg-August-Universität Göttingen, 2015.
- [44] Afra J. Zomorodian. *Topology for Computing*. Cambridge University Press, 2005.